Relation between Mixing Processes and Properties of Lithium-ion Battery Electrode-slurry

AUTHOR(S):

Takeno, Mitsuhiro; Katakura, Seiji; Miyazaki, Kohei; Abe, Takeshi; Fukutsuka, Tomokazu

CITATION:

Takeno, Mitsuhiro ...[et al]. Relation between Mixing Processes and Properties of Lithium-ion Battery Electrode-slurry. Electrochemistry 2021, 89(6): 585-589

ISSUE DATE:

2021-11-05

URL:

http://hdl.handle.net/2433/276994

Electrochemistry
The Electrochemical Society of Japan
Received: June 23, 2021
Accepted: August 12, 2021
Published online: August 19, 2021
J-STAGE https://doi.org/10.5796/electrochemistry.21-00076
Article
Electrochemistry, **89(6)**, 585–589 (2021)

Relation between Mixing Processes and Properties of Lithium-ion Battery Electrode-slurry

Mitsuhiro TAKENO,[a,b,c,§] Seiji KATAKURA,[c,*,§] Kohei MIYAZAKI,[a,§] Takeshi ABE,[a,§] and Tomokazu FUKUTSUKA[c,§]

[a] *Graduate School of Engineering, Kyoto University, Kyotodaigakukatsura, Nishikyo-ku, Kyoto 615-8510, Japan*
[b] *Energy Technology Center, Panasonic Corporation, 1-1 Matsushita-cho, Moriguchi, Osaka 570-8511, Japan*
[c] *Graduate School of Engineering, Nagoya University, Furo-cho, Chikusa-ku, Nagoya 464-8603, Japan*

* *Corresponding author: katakuras@nuee.nagoya-u.ac.jp*

ABSTRACT

The mixing process of electrode-slurry plays an important role in the electrode performance of lithium-ion batteries (LIBs). The dispersion state of conductive materials, such as acetylene black (AB), in the electrode-slurry directly influences the electronic conductivity in the composite electrodes. In this study, the relation between the mixing process of electrode-slurry and the internal resistance of the composite electrode was investigated in combination with the characterization of the electrode-slurries by the rheological analysis and the alternating current (AC) impedance spectroscopy. Some of the electrode-slurries showed higher value and gentler slope of the dynamic storage modulus in the low-angular-frequency region and higher thixotropic index than the others depending on the way of the mixing process and the AB content, agreeing with the low electronic volume resistivities of the corresponding composite electrodes and the electrode-slurries, which indicates the AB network growth. The results suggested that the low-viscosity state when AB and active electrode material are mixed contributes to the dispersive AB network.

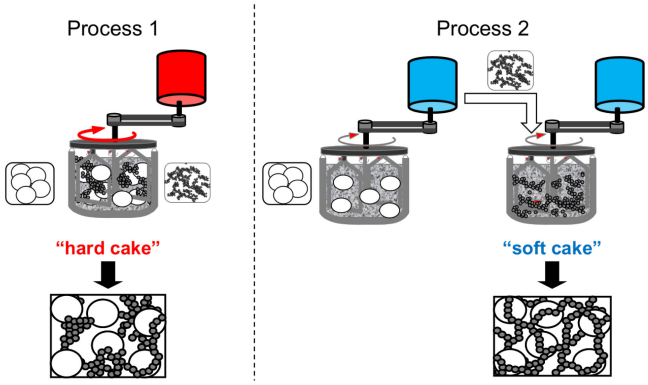

Keywords : Lithium-ion Batteries, Electrode-slurry, Mixing Process, Kneading Order

1. Introduction

In the manufacturing process of lithium-ion batteries (LIBs), an important process is a preparation of an electrode-slurry, because the electrode-slurry prepared in the initial stage determines the performances of LIBs.[1–8] The electrode-slurry is composed of active electrode material powders, conductive material powders, polymeric binders, and diluting solvents. For the fabrication of a composite electrode, the electrode-slurry is pasted on a metal foil current collector, and the solvent is dried out.

For the positive composite electrode, oxide materials such as $LiCoO_2$ are used as the active electrode material,[9–11] and carbonaceous conductive materials such as acetylene black (AB) are used to provide electronic conduction paths in the composite electrode so that the path compensate the low electronic conductivity of the oxide materials.[12] In this case, it is required that the active electrode materials and the conductive materials contact uniformly. For the fabrication of the electrode with such a uniform contact, the electrode-slurry, which is the precursor of the electrode, also has to have the uniform dispersion of the conductive materials. However, the active electrode material powders (oxide) and conductive material powders (carbon) exhibit greatly different physicochemical properties, and their uniform dispersion in the positive electrode-slurry is difficult in comparison with the electrode-slurry for the graphite negative electrode.

The components of the positive electrode-slurry are kneaded using mixers. Some studies reported that the performances of LIBs depended on the order in which the materials were injected and the mixing methods, even though the electrode-slurry has the same composition.[13–15] This indicates that the preparation procedures strongly influence the dispersion state of the electrode-slurry, which affects the performances of LIBs. Therefore, the evaluation of the electrode-slurry is important. Ligneel et al. investigated the particle distribution in the electrode-slurry using various solvents and found that a reversible capacity depended on the distribution of the conductive materials.[16] The electrode-slurry is a condensed solution containing solid phases and should be diluted to measure the particle distribution. Therefore, the dispersion state of the electrode-slurry cannot be determined directly. Rheological analysis of the electrode-slurry was carried out, and the interaction between the conductive material and the polymeric binder was discussed based on the results when carbon black was present in the polymer.[17–20] However, the dispersion state of the conductive material cannot be determined by this method. Considering the above situation, the electronic conductivity of the electrode-slurry may be the only useful indicator for determining the dispersion state of the conductive material.

§ECSJ Active Member
S. Katakura orcid.org/0000-0001-9850-727X
K. Miyazaki orcid.org/0000-0001-5177-3570
T. Abe orcid.org/0000-0002-1515-8340
T. Fukutsuka orcid.org/0000-0002-8731-9078

We have proposed a new method of measuring the electronic conductivity of the electrode-slurry by alternating current (AC) impedance spectroscopy and showed that the resulting electronic conductivity was closely related to the electrode performance in combination with rheological analysis.[21–23] After our reports, estimation of the dielectric characteristics of positive electrode-slurry was reported[24–26] and the importance of slurry control is recognized. In this study, we investigated the effect of the mixing process on the dispersion state of the electrode-slurry based on our method and discussed the relation between the electronic conduction network and the dispersion process of the conductive material.

2. Experimental

Mg-doped $LiCoO_2$ (Mg-LCO) particles (average particle size of 6.5 µm and BET surface area of 0.43 $m^2 g^{-1}$) were synthesized from a mixture of Li_2CO_3 and Co_3O_4 doped with 2 mol% Mg by a solid-state method. The obtained Mg-LCO particles were mixed with AB (average primary particle size of 40 nm), polyvinylidene difluoride (PVdF) in 1-methyl-2-pyrrolidone (NMP), and NMP using a mechanical stirrer (T.K. HIVIS MIX model 2P-03). The electrode-slurries at different AB contents were prepared at the weight ratios Mg-LCO : AB : PVdF = 97 : 1 : 2, 96 : 2 : 2, and 95 : 3 : 2 wt%, respectively. Either of the following two mixing processes (Fig. 1) was applied to prepare the electrode-slurries.

Process 1: Mg-LCO and AB were dry-mixed, and then the mixture was kneaded with NMP at 30 rpm for 30 min ("hard cake"). The "hard cake" was stirred with NMP at 95 rpm for 10 min and was then stirred with PVdF/NMP at 95 rpm for 10 min (slurry 1).

Process 2: AB was kneaded with NMP at 95 rpm for 10 min ("soft cake"). The "soft cake" was stirred with PVdF/NMP at 95 rpm for 10 min and was then stirred with Mg-LCO/NMP at 95 rpm for 10 min (slurry 2).

The obtained slurry was cast on a polyethylene terephthalate (PET) strip or aluminum foil using a doctor blade and was then heated at 80 °C for 1 h to evaporate the solvent. The loading mass was about 20 mg cm^{-2}.

The electronic volume resistivity of the composite layer on the PET strip was measured by the four-point probe method using a Loresta IP MCP-250 apparatus in compliance with JIS K7194. A direct current–internal resistance (DC–IR) test was performed using a symmetric cell. A half-cell was assembled from a composite electrode on aluminum foil (20 mm × 20 mm), lithium metal foil, an electrolyte of 1.25 mol dm^{-3} $LiPF_6$ dissolved in ethylene carbonate/ethyl methyl carbonate (1 : 3 by volume), and a microporous polyethylene separator. After the potential of the half-cell was adjusted to 3.9 V vs. Li^+/Li, the symmetric cell was assembled with two composite electrodes. Galvanostatic polarization measurements were performed using an electrochemical apparatus (Solartron 1287). The open-circuit cell voltage was measured at first, and then the cell was charged at a current of 7.2 mA for 10 s from the open circuit at various temperatures. The voltage after the current pulse was measured for 10 s. The value of DC–IR (R_{DC-IR}) was calculated from the following equation:

$$R_{DC-IR} = \frac{V_1 - V_0}{I} \quad (1)$$

where V_0 is the open-circuit voltage, V_1 is the voltage recorded at 10 s after the current pulse, and I is the current.

The electronic volume resistivity of the electrode-slurry was measured by AC impedance spectroscopy utilizing a rheometer (TA Instruments ARES) without plate rotation. The AC impedance measurements were performed using a frequency response analyzer (solartron 1260) connected to a potentiostat (solartron 1287). The detail is shown in previous paper.[17] In addition, measurements of steady-flow viscosity and dynamic viscoelastic behavior were carried out on the electrode slurry at 25 °C with a strain-controlled rheometer, and the viscosity as a function of the shear rate and the dynamic storage modulus (G') as a function of the angular frequency (ω) were determined. Cone plate fixtures with a gap angle of 0.02 rad (= 1.14 degree) and a plate diameter of 50 mm were used.

3. Results and Discussion

Figure 2 shows the electronic volume resistivity of the composite layer on PET (ρ_{vc}) against the AB content for **processes 1** and **2**. **Process 2** gave rise to a lower ρ_{vc} value than **process 1** for all AB contents. This result clearly indicated that the difference in the mixing process affected the ρ_{vc} value at the same AB content. In addition, the increase in ρ_{vc} values with a decrease in the AB content for **process 2** was smaller than that for **process 1**, which indicated the difference in the microstructure of the electrode-slurries in the two methods. To examine the microstructure of the composite electrodes, which reflects the microstructure of the electrode-slurry, scanning electron microscopy (SEM) observations were carried out.

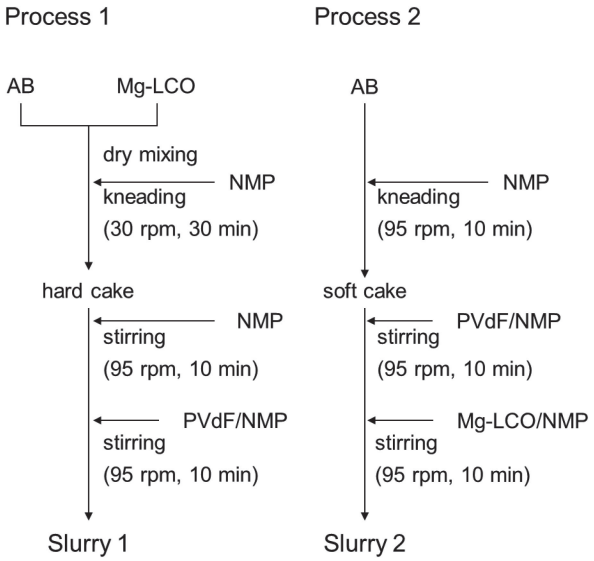

Figure 1. Schematic diagrams of the mixing process of the electrode-slurry.

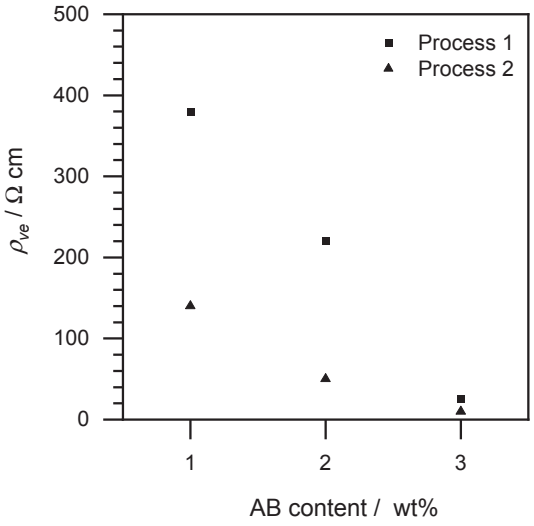

Figure 2. Electronic volume resistivity of composite layers on PET prepared by processes 1 and 2 at various AB contents.

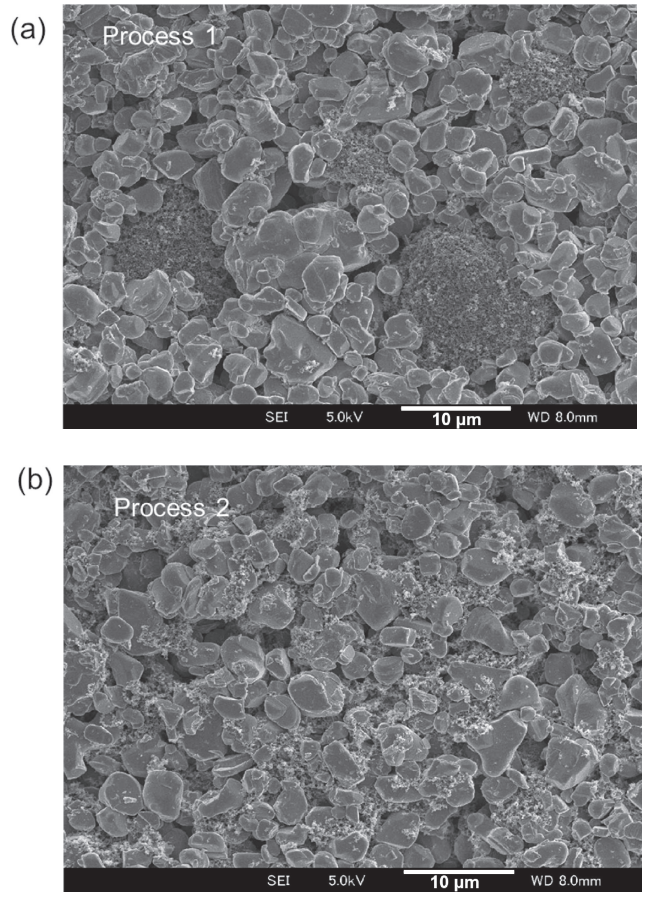

Figure 3. SEM images of composite electrodes (3 wt% AB) prepared by process 1 (a) and 2 (b).

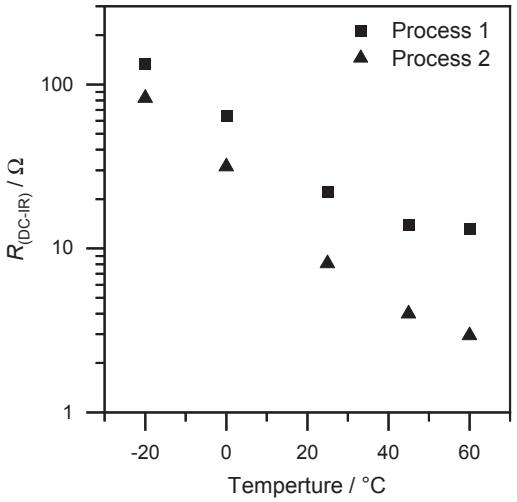

Figure 4. Temperature dependence of the R_{DC-IR} of composite electrodes (3 wt% AB) prepared by processes 1 and 2.

Table 1. Thixotropic index (TI) of various slurries.

AB (wt%)	Process 1	Process 2
1	2.6	31.2
2	4.8	13.4
3	39.5	70.5

SEM images of composite electrodes (3 wt% AB) prepared by **processes 1** and **2** are shown in Fig. 3. The large particle with a size of about 2 µm is Mg-LCO and the smaller particle is AB in the SEM images. In Fig. 3a, large clusters of AB with a size of about 10 µm are observed, and the distribution of Mg-LCO is not uniform. In contrast, AB and Mg-LCO are uniformly distributed in Fig. 3b. From the SEM images, it was confirmed that **process 2** gave a superior dispersion state of AB in the composite electrode, and this uniform dispersion state of AB contributed to the lower value of R_{DC-IR}.

Next, the influence of the difference observed in Figs. 2 and 3 on the internal resistance was examined. Figure 4 shows the R_{DC-IR} of composite electrodes (3 wt% AB) prepared by **processes 1** and **2** at various temperatures. Although the AB contents were the same, the R_{DC-IR} for **process 1** were higher than those for **process 2** at all temperatures. In addition, the difference in R_{DC-IR} increased with an increase in temperature. The activation energies obtained from the Arrhenius plots of R_{DC-IR} at −20 to 25 °C were smaller (25–30 kJ mol^{-1}) than the activation energy for interfacial lithium-ion transfer resistance.[27] Therefore, the main component of R_{DC-IR} at −20 to 25 °C is thought to be the ion transport resistance. However, temperature dependence was small in the case of **process 1** over 45 °C. This is thought to be that the main component was changed from the ion transport resistance to electronic transport resistance. In the case of **process 2**, temperature dependence was observed at the same temperature range. This difference is probably due to the different contribution of the electronic transport resistance. As shown in Fig. 2, the electronic volume resistivity of the composite layer for **process 1** was larger than that for **process 2**. In this experiment, this different electronic volume resistivity brought this different temperature dependence. It can be thought that the difference in R_{DC-IR} reflects the difference in the electronic resistance of the composite electrode. Based on this result, it was found that **process 2** gave smaller internal resistance than **process 1**, and the internal resistance was influenced by the electronic resistance of the composite electrode.

In this study, the drying process of the coated electrode-slurry was the same in both processes. Consequently, the morphological difference observed in the SEM images was thought to be due to a difference in the dispersion state of AB in the electrode-slurry. Therefore, the dispersion state of the electrode-slurry was investigated by rheological analysis and AC impedance spectroscopy. The rheological analysis indicated a shear rate dependence of the steady-flow viscosity of the electrode-slurry. Since the electrode-slurry is a solid dispersion system, it was treated as a non-Newtonian fluid.[28,29] Table 1 shows the thixotropic index (TI) determined from the steady-flow viscosity at 0.01 s^{-1} and 1 s^{-1}. In this study, TI is defined as $\eta(t = 0.01\,s^{-1})/\eta(t = 1\,s^{-1})$ since the steady-flow viscosities in the lower shear range were different in each process. The TI values increased with an increase in the AB content, and slurry 2 exhibited higher TI values than slurry 1 at all AB contents. Because a high TI indicates an increase in structural viscosity,[30] it was found that the AB network structure of the electrode-slurry grew at a high AB content, and that **process 2** promoted the growth of the AB network structure. Figure 5 shows the G' values for slurries 1 and 2. The G' of dispersed system such as an electrode-slurry indicates the mechanical properties of the network structure and AB make the network structure in this study. Therefore, G' was used to consider the network structure of AB. At the same AB content, the G' value was higher and showed gentler slope in the low-angular-frequency region for slurry 2. This result indicated that slurry 2 was more rigid than slurry 1, and an AB network structure grew in slurry 2. Slurry 2 displayed a plateau in the plot of G' in the low-angular-frequency region in the case of 1 wt% AB, which suggested the growth of an AB network structure at a low content of AB. In

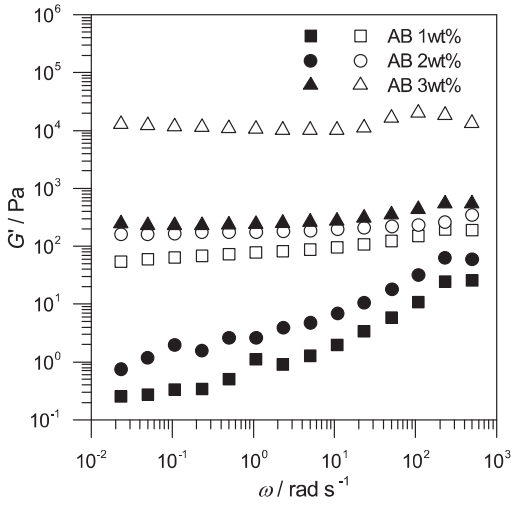

Figure 5. Dynamic storage moduli (G') of slurries 1 and 2 as a function of the angular frequency (ω). Slurry 1 is represented by closed symbols and slurry 2 is represented by open symbols.

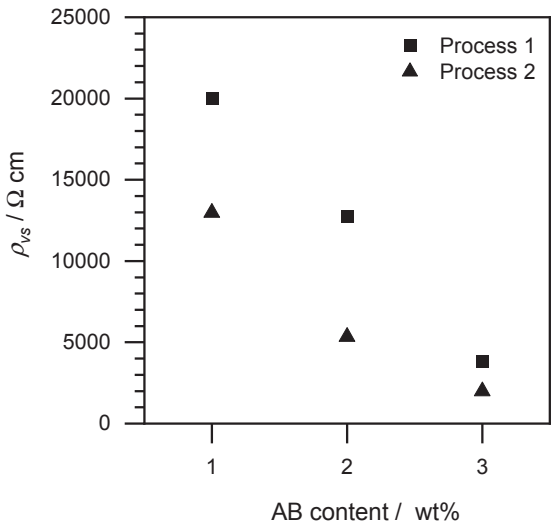

Figure 6. Electronic volume resistivities of slurries 1 and 2 at various AB contents.

contrast, for the case of slurry 1, the plateau was observed only at 3 wt% AB. This result corresponded to the increase in ρ_{vc} values at low AB contents; in other words, the AB network structure did not grow sufficiently at low AB contents in slurry 1, although the amount of AB was sufficient. The electronic volume resistivities of the electrode slurries (ρ_{vs}) for **processes 1** and **2** are shown in Fig. 6. In a similar way to the tendency of the R_{DC-IR} values, the ρ_{vs} values of slurry 2 were smaller than those for slurry 1, and their increase with a decrease in the AB content was small in slurry 2. In the case of **process 1**, the change in ρ_{vs} from 2 wt% to 3 wt% was larger than that from 1 wt% to 2 wt%. This is corresponding to the result that AB network structure grow sufficiently at 3 wt%. In the case of **process 2**, the change in ρ_{vs} from 2 wt% to 3 wt% was smaller than that from 1 wt% to 2 wt%. In Fig. 5, the G' values for slurry 2 at 3 wt% was drastically increased compared to 1 wt% and 2 wt%. Therefore, the change may be due to the too rigid AB network structure at 3 wt%, resulting in a smaller effect than expected. Based on this result, it was confirmed that the low value of R_{DC-IR} was brought about by the dispersion state of AB in the electrode slurry and that **process 2** was an effective method for dispersing AB.

Finally, we discuss the formation process of an AB network structure by the different mixing processes. In **process 1**, AB and Mg-LCO are kneaded with a small amount of NMP at first. Since the AB network is bulky and displays high oil absorptivity and large Mg-LCO particles are present at high concentrations, the addition of a large amount of NMP brings about a non-uniform wetting state. AB was dispersed at the initial stage owing to electrostatic repulsion; however, highly concentrated Mg-LCO collided with and destroyed the AB network structure, and then AB formed large clusters during kneading. As a result, the electronic resistance increased in slurry 1 and the composite electrode, which led to a large reaction distribution. As for **process 2**, AB was kneaded with NMP and then mixed with PVdF/NMP, and Mg-LCO/NMP was mixed in a low-viscosity state. As a result, the shearing force on AB was low and the AB network structure was not destroyed in slurry 2. In this way, the mixing process strongly affected the AB network structure via the difference in the viscosity of the electrode-slurry and it was found that the mixing process with LCO is important for the dispersion of AB.

4. Conclusion

In this study, the effect of the mixing processes in the preparation of the electrode-slurry on the electrode performance was investigated from the viewpoint of electronic conduction. The R_{DC-IR} values of the composite electrodes strongly depended on the mixing process at the same AB content. The electronic conductivities of the composite layer and the electrode-slurry also depended on the mixing process. From rheological analysis, it was revealed that the change in the electronic conductivity was due to the dispersion state of AB in the electrode-slurry. The simultaneous kneading of Mg-LCO and AB in NMP gave rise to low electronic conductivity owing to large clusters of AB derived from the destruction of the AB network structure in a high-viscosity state. To suppress the decrease in the electronic conductivity of the electrode-slurry, the mixing of AB/PVdF/NMP and Mg-LCO/NMP was effective owing to the low-viscosity state. On the basis of this study, a design concept for preparing electrode slurries with high electronic conductivity at a small content of AB was proposed, and this finding must be useful in the manufacture of LIBs and next-generation batteries such as all-solid-state batteries.

Acknowledgments

This work was partially supported by CREST, JST (JPMJCR12C1).

Authors Contribution

Mitsuhiro Takeno: Data curation (Lead), Investigation (Lead), Writing – original draft (Lead), Conceptualization (Lead)
Seiji Katakura: Writing – review & editing (Supporting)
Kohei Miyazaki: Writing – review & editing (Supporting)
Takeshi Abe: Project administration (Equal), Supervision (Equal), Writing – review & editing (Supporting)
Tomokazu Fukutsuka: Project administration (Equal), Supervision (Equal), Writing – review & editing (Lead)

Conflict of Interest

The authors declare that they have no conflict of interest.

Funding

Core Research for Evolutional Science and Technology: JPMJCR12C1

References

1. T. J. Patey, A. Hintennach, F. La Mantia, and P. Novák, *J. Power Sources*, **189**, 590 (2009).
2. W. Porcher, B. Lestriez, S. Jouanneau, and D. Guyomard, *J. Power Sources*, **195**, 2835 (2010).
3. W. Porcher, B. Lestriez, S. Jouanneau, and D. Guyomard, *J. Electrochem. Soc.*, **156**, A133 (2009).
4. C. C. Li, X. W. Peng, J. T. Lee, and F. M. Wang, *J. Electrochem. Soc.*, **157**, A517 (2010).
5. K. Kuratani, K. Ishibashi, Y. Komoda, R. Hidema, H. Suzuki, and H. Kobayashi, *J. Electrochem. Soc.*, **166**, A501 (2019).
6. K. Konda, S. B. Moodakare, P. L. Kumar, M. Battabyal, J. R. Seth, V. A. Juvekar, and R. Gopalan, *J. Power Sources*, **480**, 228837 (2020).
7. M. V. Duong, H. V. Nguyen, A. Garg, M. V. Tran, and P. M. L. Le, *J. Electrochem. Soc.*, **167**, 160533 (2020).
8. M. Wang, D. Dang, A. Meyer, R. Arsenault, and Y.-T. Cheng, *J. Electrochem. Soc.*, **167**, 100518 (2020).
9. Y. Takahashi, N. Kijima, K. Dokko, M. Nishizawa, I. Uchida, and J. Akimoto, *J. Solid State Chem.*, **180**, 313 (2007).
10. D. Carlier, M. Ménétrier, and C. Delmas, *J. Mater. Chem.*, **11**, 594 (2001).
11. J. Molenda and W. Kucza, *Solid State Ionics*, **117**, 41 (1999).
12. M. E. Spahr, D. Goers, A. Leone, S. Stallone, and E. Grivei, *J. Power Sources*, **196**, 3404 (2011).
13. K. M. Kim, W. S. Jeon, I. J. Chung, and S. H. Chang, *J. Power Sources*, **83**, 108 (1999).
14. C. C. Li and Y. S. Lin, *J. Power Sources*, **220**, 413 (2012).
15. G. W. Lee, J. H. Ryu, W. Han, K. H. Ahn, and S. M. Oh, *J. Power Sources*, **195**, 6049 (2010).
16. E. Ligneel, B. Lestriez, O. Richard, and D. Guyomard, *J. Phys. Chem. Solids*, **67**, 1275 (2006).
17. C. C. Li and Y. W. Wang, *J. Electrochem. Soc.*, **158**, A1361 (2011).
18. Y. Aoki, A. Hatano, and H. Watanabe, *Rheol. Acta*, **42**, 209 (2003).
19. Y. Aoki, A. Hatano, and H. Watanabe, *Rheol. Acta*, **42**, 321 (2003).
20. Y. Aoki and H. Watanabe, *Rheol. Acta*, **43**, 390 (2004).
21. M. Takeno, T. Fukutsuka, K. Miyazaki, and T. Abe, *Chem. Lett.*, **46**, 892 (2017).
22. M. Takeno, T. Fukutsuka, K. Miyazaki, and T. Abe, *Carbon*, **122**, 202 (2017).
23. M. Takeno, T. Fukutsuka, K. Miyazaki, and T. Abe, *J. Electrochem. Soc.*, **164**, A3862 (2017).
24. Z. Wang, T. Zhao, and M. Takei, *J. Electrochem. Soc.*, **164**, A2268 (2017).
25. Z. Wang, T. Zhao, and M. Takei, *J. Electrochem. Soc.*, **166**, A35 (2019).
26. Z. Wang, T. Zhao, M. Kanzawa, K. Liu, and M. Takei, *Trans. Inst. Meas. Control*, **42**, 704 (2020).
27. N. Ogihara, S. Kawauchi, C. Okuda, Y. Itou, Y. Takeuchi, and Y. Ukyo, *J. Electrochem. Soc.*, **159**, A1034 (2012).
28. V. M. Lobe and J. L. White, *Polym. Eng. Sci.*, **19**, 617 (1979).
29. G. J. Osanaiye, A. I. Leonov, and J. L. White, *J. Non-Newton. Fluid*, **49**, 87 (1993).
30. M. Mooney, *J. Colloid Sci.*, **6**, 162 (1951).